Mechanical deformation of carbon nanotube nano-rings on flat substrate

Meng Zheng and Changhong Ke[a)]
Department of Mechanical Engineering, State University of New York at Binghamton, Binghamton, New York 13902, USA

(Received 30 September 2010; accepted 10 January 2011; published online 5 April 2011)

We present a numerical analysis of the mechanical deformation of carbon nanotube (CNT) nano-rings on flat graphite substrates, which is motivated by our recent experimental findings on the elastic deformation of CNT nano-rings. Our analysis considers a perfectly circular CNT ring formed by bending a straight individual or bundled single-walled nanotube to connect its two ends. The seamless CNT ring is placed vertically on a flat graphite substrate and its respective deformation curvatures under zero external force, compressive, and tensile forces are determined using a continuum model based on nonlinear elastica theory. Our results show that the van der Waals interaction between the CNT ring and the substrate has profound effects on the deformation of the CNT ring, and that the interfacial binding interaction between the CNT ring and the substrate is strongly modulated by the ring deformation. Our results demonstrate that the CNT ring in force-free conditions has a flat ring segment in contact with the substrate if the ring radius $R \geq \sqrt{\frac{EI}{2W_{vdw}}}$, in which EI is the flexural rigidity of the nanotube and W_{vdw} is the per-unit-length van der Waals energy between the flat ring segment and the substrate. Our results reveal that the load-deformation profiles of the CNT ring under tensile loadings exhibit bifurcation behavior, which is ascribed to its van der Waals interaction with the substrate and is dependent on its relaxed conformation on the substrate. Our work suggests that CNT nano-rings are promising for a number of applications, such as ultrasensitive force sensors and stretchable and flexible structural components in nanoscale mechanical and electromechanical systems. © *2011 American Institute of Physics*. [doi:10.1063/1.3554406]

I. INTRODUCTION

Carbon nanotube (CNT) closed-ring type structures have been reported in both as-grown and posttreated samples. CNT nano-rings formed by individual or bundled single-walled and multi-walled carbon nanotubes have been synthesized directly using the laser ablation[1] and chemical vapor deposition (CVD)[2] methods. The CNT nano-ring can be also formed through folding a long nanotube fiber either by partially overlapping itself[3–5] or by having its two prefunctionalized ends connected.[6] The self-folding formation of circular structures is due to the fact that the bending in the nanotube is balanced by the van der Waals (*vdw*) interaction between contacting nanotube surfaces. The CNT folding process can be facilitated by ultrasonic agitations[7,8] and surface chemical functionalization.[9–11]

The formation mechanism and the stability of CNT nano-rings have been theoretically investigated by a variety of modeling techniques, including tight-binding and semiempirical quantum mechanics,[12] molecular dynamics,[13–19] continuum mechanics,[16,20] and thermodynamics.[21] From these theoretical studies, two nanotube ring formation mechanisms are proposed. The nano-ring can be formed by either pure hexagon networks or a hexagon structure with pentagon-heptagon defects. It is reported that, for nano-rings with large ring diameters, the pure hexagon structure is energetically more stable and the ring curvature is accommodated by the bending of the nanotube. For nano-rings with small ring diameters, the mixture of hexagon networks and pentagon-heptagon defects is energetically more favorable with the ring curvature accommodated by pentagon-heptagon defects. It is also observed that buckling and ripples may be formed in nanotube rings, which are closely related to the respective diameters of the ring and the tube. The critical nanotube length that is required to form a perfectly circular ring structure is found to increase with diameter. Nanotubes with smaller diameters will form perfect ring structures for smaller tube lengths.

Because CNTs are considered one of the strongest and most flexible materials as a result of the C-C covalent bonding and the seamless hexagonal network architecture, CNT nano-rings hold great potential for a number of applications such as flexible and stretchable load-bearing structural components in nanoscale systems. For the pursuit of such applications, it is imperative to understand the elastic behavior of the CNT nano-ring, in particular, when it is in contact with other surfaces or substrates. However, the mechanical deformation of CNT rings under external loadings has been little explored either theoretically[19] or experimentally.[22] Only very recently, the mechanical deformation of carbon nanotube nano-rings against a flat substrate under both compressive and tensile loadings were experimentally characterized by our group using in situ nanomanipulation techniques inside a high-resolution scanning electron microscope.[22] Our experimental results clearly show that the CNT nano-ring possesses purely elastic behavior in both tension and

[a)]Electronic mail: cke@binghamton.edu

compression within the large displacement deformation regime. Our experimental results also reveal that the *vdw* interaction between the nanotube ring and the substrate has profound impacts on its mechanical deformation. Partially motivated by our experimental observation of the mechanical deformation of nanotube nano-rings, in this paper we present a numerical analysis of the mechanical deformation of CNT nano-rings in contact with flat substrates using a continuum model based on nonlinear elastica theory. Our model takes into account the *vdw* interaction between the nano-ring and the substrate and reveals its respective elastic deformation curvatures in force-free conditions, and under compressive and tensile loadings.

II. MODELING

In this section, we present a continuum model based on nonlinear elastica theory to study the mechanical deformation of the CNT ring. In our model, the CNT circular ring is formed by bending a long and straight single-walled carbon nanotube (SWNT) to connect its two ends, thus the ring curvature is accommodated by the bending moment in the nanotube. The nanotube segment is theoretically modeled as an inextensible elastica rod.[23–25] This modeling assumption is consistent with the previous experimental observation that carbon nanotubes could be repeatedly bent to large angles and strain with no permanent distortion of the tube topography.[26] In our modeling, we consider that the radius of the CNT ring is significantly larger than that of the CNT by more than one order of magnitude. Considering that the stiffness of a circular structure is inversely proportional to the third power of its radius,[27] the nanotube radial deformation is considered to be negligible in our analysis and the nanotube circular cross section is assumed to remain intact during the ring deformation process because the cross-section stiffness of the nanotube is more than three orders of magnitude higher than that of the CNT ring. In our model, we consider the mechanical deformation of the nanotube ring in contact with a N_0-layer graphite sheet (a) in force-free conditions (zero external force), (b) under compressive pushing force, and (c) under tensile pulling force, as illustrated in Figs. 1(a)–1(c), respectively. The considered external point load applied on the CNT ring is consistent with our experimental measurements and is of generality when the CNT ring is used as a force sensor or load bearing structural component in nanoscale mechanical systems. It is noted that the analysis presented in this paper for this load type can be readily extended to other types of loads (e.g., distributed loads).

Due to the *vdw* interaction between the CNT ring and the substrate, a flat ring segment may come into being on the contact interface with the substrate. As shown in our later analysis, the existence of the flat ring segment is dependent on the strength of the *vdw* interaction and the flexural rigidity of the CNT ring segment. Only if the nanotube ring radius is smaller than a threshold value will the ring keep its perfectly circular shape when it stands on the substrate. The diagram of a CNT ring of a flat contact with the substrate under an external load P is illustrated in Fig. 2(a). The free-body diagram of the ring segment DG is schematically shown in Fig. 2(b). Symmetry allows us to study one-half of the configuration, i.e., $0 \le s \le l$, where s is the arc length starting from point D, and l is one-half of the length of the ring segment in the noncontact region. The inextensible condition gives $a + l = \pi R$, in which a is one-half of the length of the ring flat segment, and R is the ring radius. In the free-body diagram as shown in Fig. 2(b), T, V, and M represent the tension, shear, and bending moment on the nanotube cross-section at s, respectively. The reaction tension, shear, and bending moment at D ($s = 0$) are denoted as T_D, V_D, and M_D, respectively. From the symmetry, we can easily obtain that the shear force V_D at $s = 0$ equals to one-half of the external force P, i.e., $V_D = \frac{P}{2}$.

A. Ring–substrate interaction

We use a continuum model to calculate the *vdw* interaction between the CNT ring and the substrate based on the Lennard–Jones (*L–J*) potential, which defines the potential between two atoms as $\phi = \frac{C_{12}}{r^{12}} - \frac{C_6}{r^6}$ in which r is the interatom distance, and C_6 and C_{12} are material constants (for carbon–carbon interactions, $C_6 = 15.2$ eV Å^6 and $C_{12} = 24.2$ KeVÅ^{12}). The per-unit-length *vdw* energy between a single-walled nanotube and an in-parallel N_0-layer graphite sheet is given by[28]

$$W_{vdw} = \pi R_{CNT}\sigma^2 \sum_{N=1}^{N_0} \times \left\{ \int_{-\pi}^{\pi} \left(\frac{C_{12}}{5[r_0 + d_0(N-1) + R_{CNT}(1+\sin\beta)]^{10}} - \frac{C_6}{2[r_0 + d_0(N-1) + R_{CNT}(1+\sin\beta)]^4} \right) d\beta \right\} \quad (1)$$

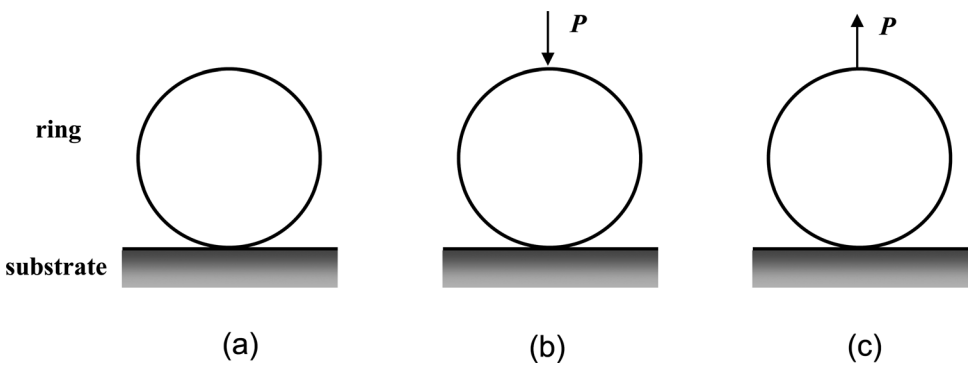

FIG. 1. Schematics of a circular CNT ring in contact with a flat substrate under (a) zero external force; (b) a compressive point force; (c) a tensile point force.

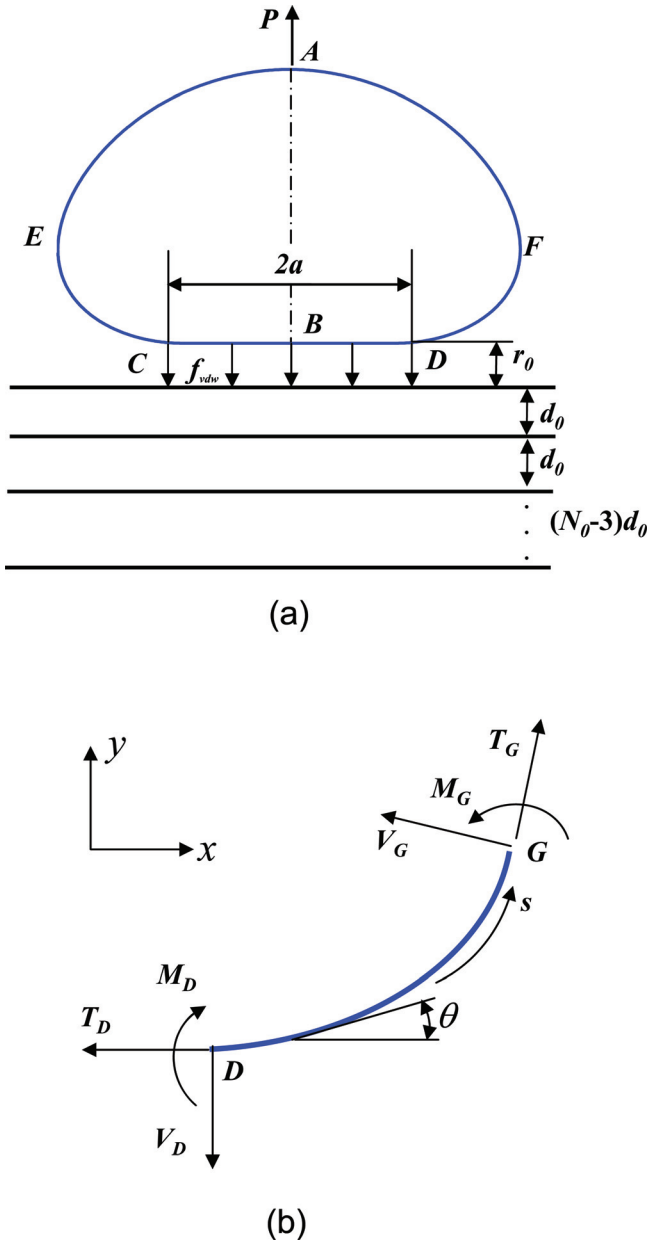

FIG. 2. (Color online) (a) Schematic of a CNT ring of a flat ring segment in contact with a N_0-layer graphite substrate under a tensile force P; (b) the free-body diagram of a ring segment.

where $\sigma = 38/\text{nm}^2$ is the graphene surface density, R_{CNT} is the nanotube radius, r_0 is the distance between the bottom atom of the CNT cross section and the top graphene layer of the graphite substrate, and $d_0 = 0.335$ nm is the graphene interlayer distance. It is noted that the per-unit-length *vdw* force $f_{vdw} = \frac{dW_{vdw}}{dr_0}$.

When the CNT has a flat ring segment in contact with the substrate, we assume that the *vdw* interaction between the noncontact portion of the ring and the substrate is negligible,[29] and only consider the *vdw* interaction in the flat contact region. In the flat contact region, the contact between the CNT ring and the substrate is under a quasistatic balance between the elastic deformation of the ring segment and the *vdw* interaction, meaning that the *vdw* interaction-based adhesion between the CNT ring and the substrate has to balance the bending moment in the ring segment at point D.[30,31] Therefore, the equilibrium conditions give

$$V_D = f_{vdw}(r_0)\, a = \frac{P}{2} \tag{2}$$

$$W_{vdw}(r_0) = \frac{M_D^2}{2EI} \tag{3}$$

where E and I are the Young's modulus and the moment of inertial of nanotubes, respectively. For SWNTs, the moment of inertial $I = \frac{\pi}{4} R_{CNT}^4$

B. Elastica model

For the nonlinear elastica model, we introduce the following dimensionless quantities: $\bar{s} = \frac{s}{R}$, $\bar{x} = \frac{x}{R}$, $\bar{y} = \frac{y}{R}$, $\bar{T} = \frac{T}{EI/R^2}$, $\bar{V} = \frac{V}{EI/R^2}$, $\bar{M} = \frac{M}{EI/R}$, $\bar{P} = \frac{P}{EI/R^2}$, and $\bar{a} = \frac{a}{R}$. The deformation of the CNT ring is given by

$$\frac{d^2\theta}{d\bar{s}^2} = \bar{T}\sin\theta - \bar{V}\cos\theta, \tag{4}$$

where θ is the angle between the tangent of the ring segment at s and the x-axis. At point D ($s = 0$), $\bar{x}_D = \bar{a}$, $\theta_D = 0$ and $\frac{d\theta}{d\bar{s}}\big|_D = \bar{M}_D$. By integrating Eq. (4), we obtain,

$$\frac{d\theta}{d\bar{s}} = \pm\sqrt{2\bar{T}_D(1-\cos\theta) - \bar{P}\sin\theta + \bar{M}_D^2}. \tag{5}$$

For the CNT ring under pulling forces or zero external force, it is clear that $\frac{d\theta}{d\bar{s}} \geq 0$ for $0 \leq \theta \leq \pi$. For the CNT ring in compression, an inflection point may exist in its deformation curvature, which is denoted as (s^*, θ^*) in the (s, θ) coordinate system. These two cases are analyzed separately in the following sections.

1. CNT ring under zero external force or under tensile forces

From integrating Eq. (5), we obtain

$$\bar{s}(\theta) = \int_0^\theta \frac{1}{\sqrt{2\bar{T}_D(1-\cos\theta) - \bar{P}\sin\theta + \bar{M}_D^2}}\,d\theta. \tag{6}$$

Considering $d\bar{x} = \cos\theta\, d\bar{s}$ and $d\bar{y} = \sin\theta\, d\bar{s}$, Eq. (6) gives

$$\bar{x}(\theta) = \int_0^\theta \frac{\cos\theta}{\sqrt{2\bar{T}_D(1-\cos\theta) - \bar{P}\sin\theta + \bar{M}_D^2}}\,d\theta + \bar{a} \tag{7a}$$

$$\bar{y}(\theta) = \int_0^\theta \frac{\sin\theta}{\sqrt{2\bar{T}_D(1-\cos\theta) - \bar{P}\sin\theta + \bar{M}_D^2}}\,d\theta. \tag{7b}$$

The boundary conditions at point A are $\bar{x}_A = 0$, $\theta_A = \pi$, and $\bar{s}_A = \pi - \bar{a}$. Therefore,

$$\int_0^\pi \frac{\cos\theta}{\sqrt{2\bar{T}_D(1-\cos\theta) - \bar{P}\sin\theta + \bar{M}_D^2}}\,d\theta = -\bar{a} \tag{8a}$$

$$\int_0^\pi \frac{1}{\sqrt{2\bar{T}_D(1-\cos\theta) - \bar{P}\sin\theta + \bar{M}_D^2}}\,d\theta = \pi - \bar{a}. \tag{8b}$$

The deformation curvature of the CNT ring can be obtained by solving the equation set including Eqs. (2), (3), (8a), and (8b).

This equation set involves four unknown variables, r_0, $\bar{a}$, $\bar{T}_D$, and $\bar{M}_D$, and can be solved efficiently using a shooting method.

When no external force is applied on the CNT ring, i.e. $P=0$, the relaxed conformation of the CNT ring on the substrate is determined by the flexural rigidity of the nanotube and its *vdw* interaction with the substrate. From Eq. (8b), we obtain

$$\int_0^{\pi} \frac{1}{\sqrt{2\bar{T}_D\,(1-\cos\,\theta\,)+\bar{M}_D^2}}\mathrm{d}\theta \;=\; \pi \;-\; \bar{a}. \qquad (9)$$

The reaction force $\bar{T}_D \to 0$ as the contact length between the CNT ring and the substrate tends to be very small. Therefore, if the CNT ring has a flat ring segment in contact with the substrate (i.e., $\bar{a}>0$), the following condition has to be satisfied, $\bar{M}_D^2 \;>\; 1$. This result shows that the critical ring radius for the CNT ring to have a flat contact with the substrate, $R_{cr}^{\ \mathrm{flat}}$, is given by

$$R_{cr}^{\mathrm{flat}} \;=\; \sqrt{\frac{EI}{2W_{vdw}}} \qquad (10)$$

It is noted that similar phenomena have been reported in prior studies of the radial deformation of individual SWNTs on a flat substrate[32] or between two neighboring SWNTs[29] that are purely due to the *vdw* interaction. The reason that the CNT ring may remain as a perfectly circular structure on a flat substrate is due to the fact that the CNT ring employed in our study is not internal force-free for its undeformed configuration and an internal bending moment is accommodated by its circular ring conformation.

2. CNT ring under compressive forces

When the CNT ring is pushed against the substrate under compressive forces, inflection points may develop in the curvature of the deformed CNT ring. The slope of the CNT ring curvature in the $(s,\,\theta)$ coordinate system, i.e., $\frac{\mathrm{d}\theta}{\mathrm{d}s}$, changes from positive to negative around the inflection point $(s^*,\,\theta^*)$, while at the inflection point $\frac{\mathrm{d}\theta}{\mathrm{d}s}=0$. From Eq. (5), we obtain,

$$2\bar{T}_D\,(1-\cos\,\theta^*)-\bar{P}\,\sin\,\theta^*\,+\,\bar{M}_D^2\;=\;0. \qquad (11)$$

The deformation curvature of the CNT ring in compression without inflection points can be obtained by solving the equation sets for CNT rings in tension, as presented in Sec. II.B.1. The deformation curvature of the CNT ring in compression with inflection points is given by

$$\int_0^{\theta^*} \frac{\cos\theta}{\sqrt{2\bar{T}_D\,(1-\cos\,\theta)-\bar{P}\,\sin\,\theta+\bar{M}_D^2}}\mathrm{d}\theta - \int_{\theta^*}^{\pi} \frac{\cos\theta}{\sqrt{2\bar{T}_D\,(1-\cos\,\theta\,)-\bar{P}\,\sin\,\theta+\bar{M}_D^2}}\mathrm{d}\theta \;=\; -\bar{a} \qquad (12a)$$

$$\int_0^{\theta^*} \frac{1}{\sqrt{2\bar{T}_D\,(1-\cos\,\theta)-\bar{P}\,\sin\,\theta+\bar{M}_D^2}}\mathrm{d}\theta - \int_{\theta^*}^{\pi} \frac{1}{\sqrt{2\bar{T}_D\,(1-\cos\,\theta\,)-\bar{P}\,\sin\,\theta+\bar{M}_D^2}}\mathrm{d}\theta \;=\; \pi \;-\; \bar{a}. \qquad (12b)$$

The boundary conditions at points D and A are $\bar{x}_D \;=\; \bar{a}$, $\bar{y}_D \;=\; 0$, $\bar{x}_A \;=\; 0$, $\theta_A=\pi$. The deformation curvature of the CNT ring in compression with inflection points can be obtained by numerically solving the equation set that consists of Eqs. (2), (3), (11)–(12) and that involves five unknown variables, θ^*, r_0, $\bar{a}$, $\bar{T}_D$, and $\bar{M}_D$.

For the CNT ring in compression, tension, or force-free conditions, the total potential energy of the system is given by

$$U \;=\; 2\int_0^{l} \frac{EI}{2}\left(\frac{d\theta}{ds}\right)^2 \mathrm{d}s \;-\; 2aW_{vdw} \;-\; P\Delta y_A, \qquad (13)$$

where the first term is the strain energy stored in the deformed CNT ring, the second term is the *vdw* energy between the CNT ring and the substrate, and the third term is the work done by the external force [Δy_A is the vertical displacement of point A in Fig. 2(a)]. The dimensionless potential energy is given by $\bar{U} \;=\; \frac{U}{EI/R}$.

3. The applicable range of the elastica model

The elastica model presented in the previous sections is based on nanotube rings of perfectly circular geometry. Prior continuum and atomistic modeling studies have shown that the CNT in a ring structure can buckle and the ring actually becomes polygon shapes,[16,18] which is due to the fact that the deformation of the carbon network in the CNT can not be accommodated by the smooth circular curvature of the ring. The buckling of the CNT ring largely depends on the ratio between the ring radius R and the nanotube radius R_{CNT}. Therefore, it is of importance to identify the applicable range of the elastica model in term of the geometrical parameters of the CNT ring. Based on the work reported by Hod *et al.*,[16] the critical CNT ring radius for the ring to keep an unbuckled and perfectly circular shape is given by

$$R_{cr}^{\mathrm{buckle}} \;=\; \frac{{n_{cr}}^2}{2}\,R_{CNT} \qquad (14)$$

where n_{cr} is the minimal integer for a perfectly circular ring structure and can be obtained based on atomistic simulations.

It is noted that the buckling of the CNT ring is dependent on the chirality of the nanotube that determines the tube radius.[33] We consider two representative types of single-walled carbon nanotubes, namely arm-chair $(m,\,m)$ and zig-zag $(m,\,0)$ nanotubes, in which m is the chiral vector index. The dependences of the critical ring radii $R_{cr}^{\ \mathrm{flat}}$ and $R_{cr}^{\ \mathrm{buckle}}$ on the tube radius for both arm-chair and zigzag nanotubes are shown in Figs. 3(a) and 3(b), respectively. For arm-chair tubes we use $n_{cr}=8$ and for zig-zag tubes we use $n_{cr}=13$ in the calculation of $R_{cr}^{\ \mathrm{buckle}}$, which are presented in the circle curves in Figs. 3(a) and 3(b), and are consistent with the data (diamond curves) from the molecular dynamic (MD) simulation reported in Ref. 33. For both types of tubes, our results show that $R_{cr}^{\ \mathrm{buckle}} > R_{cr}^{\ \mathrm{flat}}$ for the indicated nanotube radius range. Therefore, the region above the circle/diamond curves in both Figs. 3(a) and 3(b) corresponds to an unbuckled CNT ring at a flat contact with the substrate. Because accurate

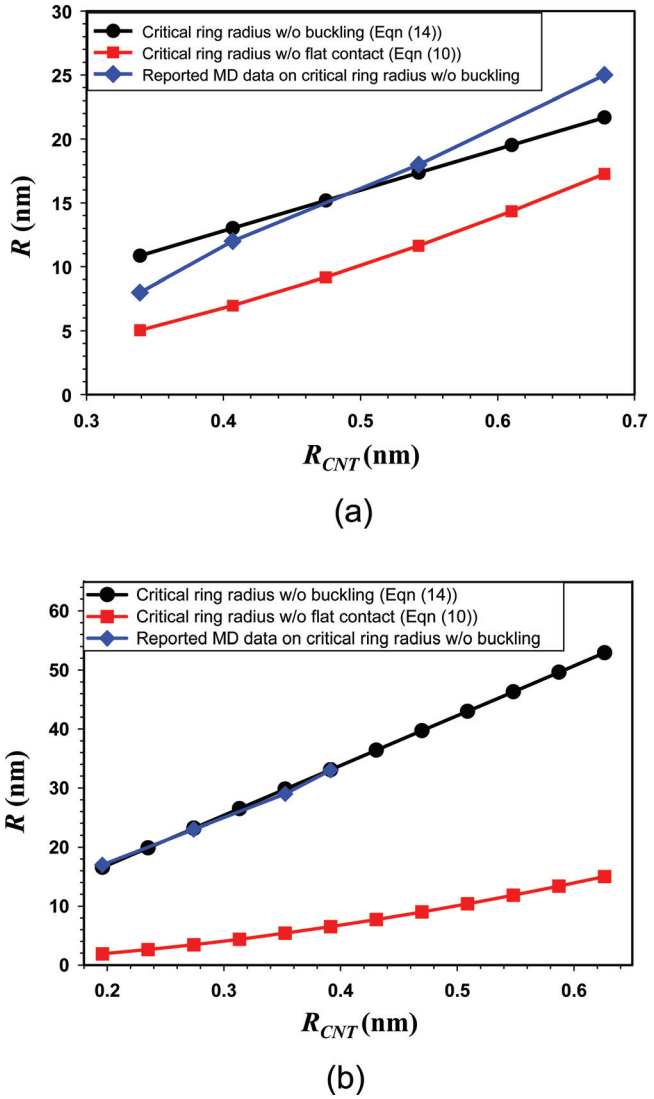

FIG. 3. (Color online) Dependences of the critical ring radii for a CNT ring of no flat contact with the substrate (red-square curve) and of no buckling (black-circle curve) on the nanotube radius based on the predictions using the continuum models. The blue-diamond points represent the reported MD data about the buckling of the CNT ring in Ref. 33. Data shown in (a) are for arm-chair nanotubes; while data shown in (b) are for zig-zag nanotubes.

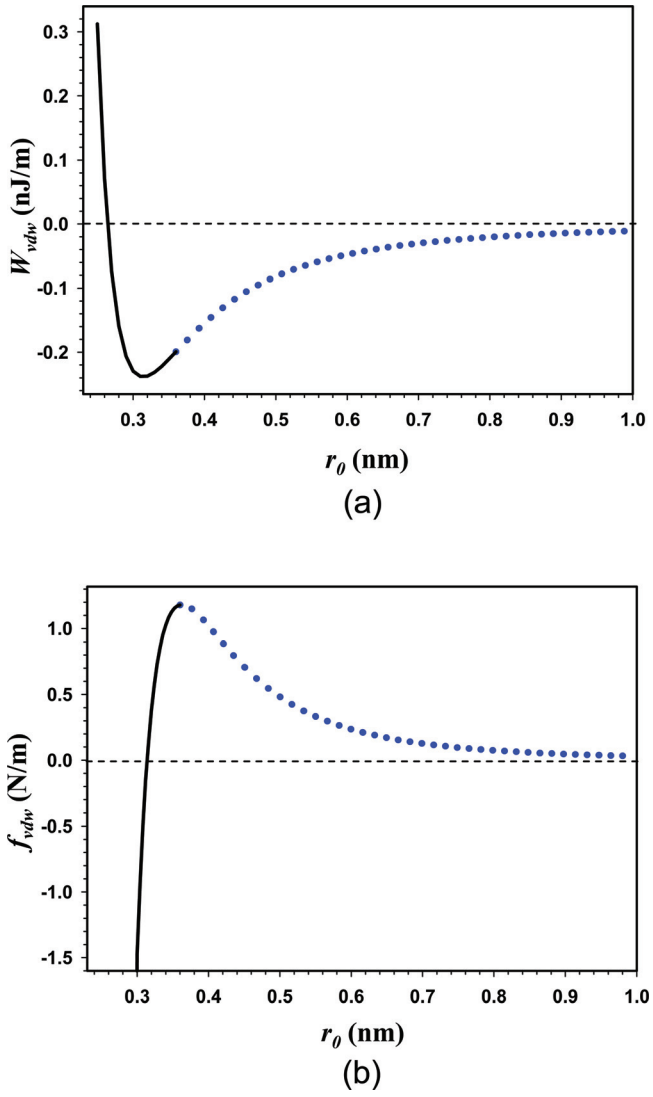

FIG. 4. (Color online) The dependence of the per-unit-length van der Waals energy (a) and force (b) between a straight (10, 10) SWNT segment and a 40-layer graphite sheet on the gap distance.

modeling of the buckling of the CNT ring requires the consideration of the microscopic structure of the nanotube, it may be only properly treated using atomistic-level modeling techniques. In this study, we only consider CNT rings with geometrical parameters in the unbuckled configuration range.

III. RESULTS AND DISCUSSION

To illustrate mechanical deformation of the CNT ring as presented in Sec. II, we consider a CNT ring formed by bending a straight arm-chair (10,10) SWNT to connect its two ends and form a closed circular structure. This CNT ring is vertically placed on a 40-layer graphite sheet. The radius of the (10,10) SWNT is 6.78 Å.[34] The axial elastic strength of the CNT is ascribed to the covalent C-C bonding, and the Young's modulus of the nanotube $E = 1$ TPa is employed in the simulation.[35] Figures 4(a) and 4(b) show W_{vdw} and f_{vdw} for a straight (10,10) tube segment above a 40-layer graphite sheet at different gap distance r_0, respectively. It is noticed that the f_{vdw} plot displays a bifurcation in the attractive force zone, while displaying a simple monotonous profile in the repulsive force zone. The solid segment of the *vdw* force curve that has positive slope indicates that the *vdw* force increases with the gap, while the *vdw* force decreases with the increase of the gap for the dotted segment.

The equilibrium gap distance between the nanotube segment and the top graphene sheet is found to be 3.144 Å based on Eq. (1), which is in good agreement with the value (3.152 Å) obtained by using a full atomistic model that sums up the *vdw* interaction between each pair of carbon atoms on the CNT and the graphite sheet. It is noted that this equilibrium gap distance is smaller than that of two parallel single-layer graphene sheets, which was reported to be in the range of 0.34∼0.35 nm.[29,34,36,37]

On the basis of Fig. 3(a), a CNT ring of 0.678 nm in tube radius and 40 nm in ring radius has a flat ring segment in contact with the substrate and does not buckle. The relaxed deformation curvature of this CNT ring on the

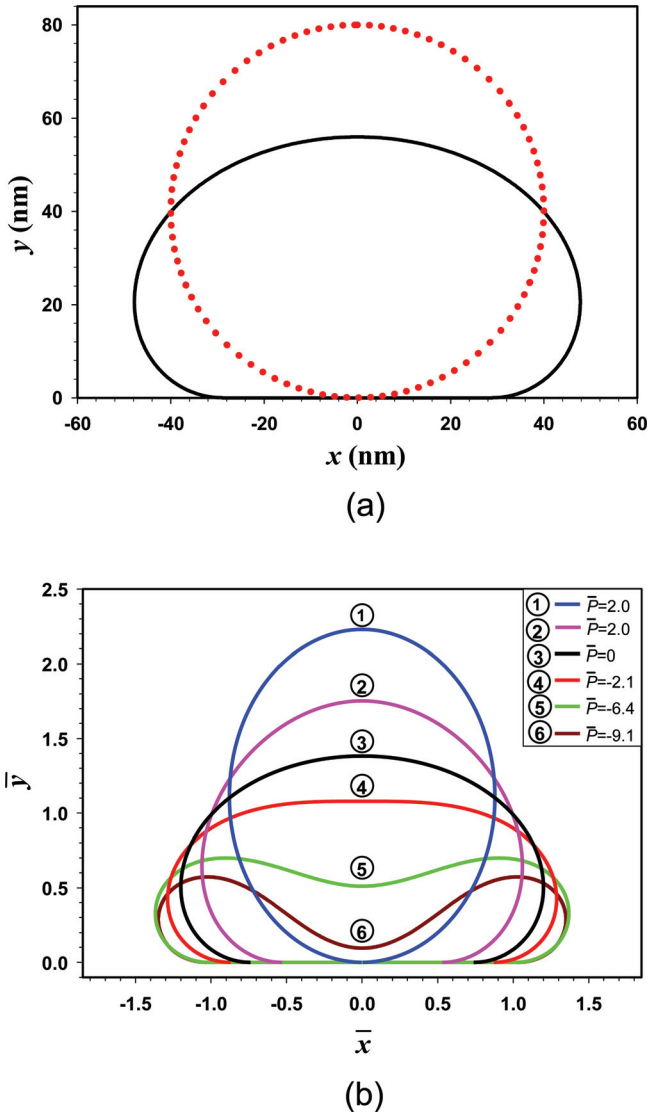

FIG. 5. (Color online) (a) Comparison between the relaxed deformation curvature (black-solid curve) and the original conformation (red-dotted curve) of a CNT circular ring of 40-nm in ring radius standing on the graphite substrate with zero external force. (b) Representative deformation curvatures of the CNT ring shown in (a) under a variety of tensile and compressive loads.

graphene sheet in the force-free condition (i.e., $P=0$) is presented as the solid curve in Fig. 5(a), which is contrasted with its original circular shape as shown in the dotted curve. The width of the flat ring segment, $2a$, and the height of the deformed ring, $\overline{AB}$, are calculated to be 59.1 nm and 55.3 nm, respectively. The per-unit-length *vdw* energy at the flat contact region $W_{vdw}=0.27$ nJ/m. These results clearly show that the *vdw* interaction between the CNT ring and the substrate has a substantial effect on the ring deformation, even in external force-free conditions.

Using the nonlinear elastica model presented in Sec. II, we determine the deformation curvatures of the CNT ring under both compressive and tensile loadings. Selected deformation curvatures of the CNT ring at various applied forces are presented in Fig. 5(b). Our results show that the flat ring segment becomes shorter when the ring is subject to tensile loadings and, at the same time, the height of the CNT ring becomes longer and the width of the CNT ring, $\overline{EF}$, becomes smaller. When the CNT ring is subject to compressive loadings, two distinct deformation configurations occur, depending on the magnitude of the load. For small compressive loads, the overall deformation curvature of the CNT ring does not change dramatically from its relaxed conformation and the slope of the deformation curvature in the (s, θ) coordinate system remains nonnegative, as exemplified by curve 4 ($\bar{P}=-2.1$) shown in Fig. 5(b). In such a loading regime, both the width of the CNT ring and the contact length between the ring and the substrate increase with the load, while the height of the ring decreases with the increase of the load. When the applied compressive load exceeds a certain value, inflection points show up in the deformation curvature of the CNT ring. The slope of the deformation curvature changes sign at the inflection point from positive to negative, then the slope becomes zero at point A. For such loading conditions, the curvature of the deformed CNT ring displays a concavity, as exemplified by curve 5 ($\bar{P}=-6.4$) and curve 6 ($\bar{P}=-9.1$) in Fig. 5(b). The comparison between curves 5 and 6 in Fig. 5(b) show that the width of the deformed CNT ring actually decreases with the increase of the load, contrasting with the width increase under the small compressive load. Figures 6(a)–6(f) show the respective dependences of six pertinent parameters of the ring deformation on the applied load, including (a) the ring height, (b) the width of the flat ring segment, (c) the gap distance between the ring flat segment and the substrate, (d) the potential energy of the system, (e) the axial tensile force in the nanotube at point D, and (f) the bending moment in the nanotube at point D. It is noticed that all the plots in Fig. 6 display bifurcation behavior when the CNT ring is subject to tensile loading, while displaying monotonous curves when the CNT ring is in compression. The bifurcation indicates that one tensile load corresponds to two equilibrium ring deformation configurations, which are respectively represented by the square and the circle branches in Figs. 6(a)–6(f). This bifurcation is due to the fact that the *vdw* interaction displays a bifurcation in the attractive-force regime, as shown in Fig. 4(b). The square and circle branches in Figs. 6(a)–6(f) correspond to the *vdw* interaction as shown by the solid and the dotted segments in Figs. 4(a) and 4(b), respectively. Under the same tensile load, the height of the deformed CNT ring is higher for the circle branch of the bifurcation, while the length of the flat contact between the CNT ring and the substrate is longer for the square branch. It is noted that the length of the flat contact as shown by the circle branch is in the sub-nm regime, implying a nearly point contact between the CNT ring and the substrate. This difference is also clearly shown through the comparison between curves 1 and 2 in Fig. 5(b). The total potential energy of the system as presented in Fig. 6(d) reveals that the total potential energy of the circle branch is always higher than that of the square branch. Our analysis shows that the deformation curvatures of the CNT ring represented by the square branch of the bifurcation are stable equilibrium configurations, while the circle branch represents unstable equilibrium configurations. Fig. 6(e) shows that the ring segment in contact with the substrate is actually under compressive axial force, which is opposite to the initial tension force assumption shown in Fig. 2(b).

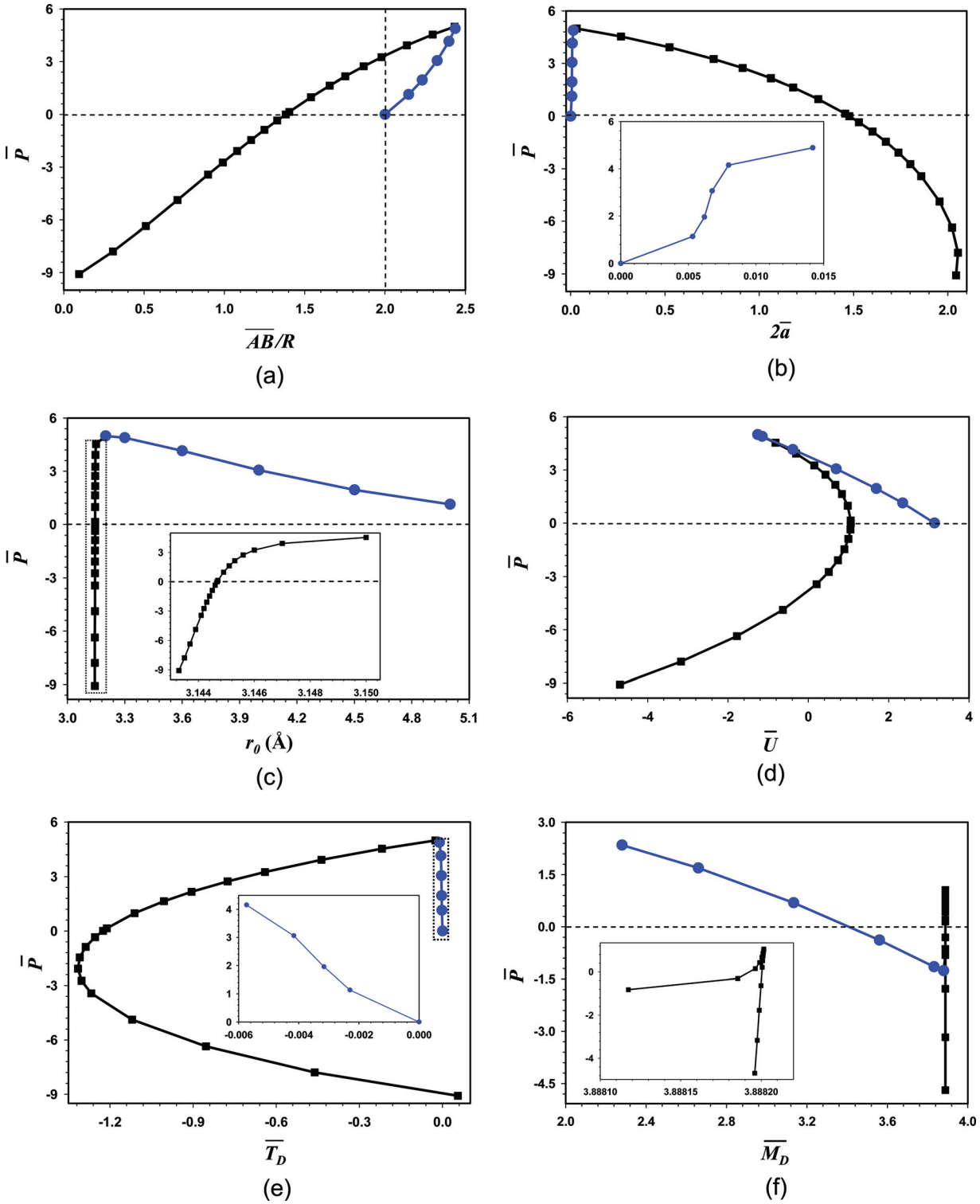

FIG. 6. (Color online) The respective dependences of six pertinent quantities about the CNT ring deformation on the applied load: (a) the CNT ring height, (b) the length of the flat ring segment, (c) the gap distance between the ring flat and the substrate, (d) the total potential energy in the system, (e) the axial force in the CNT ring segment at point *D*, and (f) the bending moment in the CNT ring segment at point *D*. The black-square branches represent the stable ring deformation configurations, while the blue-circle branches represent the unstable ring deformation configurations.

The compressive axial force transits to tensile force only when a significant external compressive load is applied on the CNT ring.

It is noted that the external load equals the product of the contact length $2a$ and the per-unit-length *vdw* force f_{vdw}, the latter of which is determined by the gap distance r_0. The square branch in Fig. 6(b) shows that the magnitude of the pulling force is inversely correlated with contact length and that the maximum pulling force occurs at a very small contact length, while the magnitude of the pushing force in general is positively correlated with the contact length. There is a very small variation of the gap distance between the CNT ring and the substrate as shown by the square curve in Fig. 6(c). The external load corresponding to the maximum

f_{vdw} is actually much smaller than the maximum external force as a result of the very small contact length. This observation suggests that the change of contact length between the nanotube ring and the substrate is a gradual pull-off or push-on process, which is strongly modulated by the deformation of the CNT ring that has a very low stiffness.

Figure 6(a) shows that the height of the deformed CNT ring displays a nearly linear relationship with the applied compressive load for $\bar{P}$ ranging from 0 to −6.4 and the corresponding ring height $\overline{AB}$ from $1.4R$ to $0.5R$. We define the stiffness or the spring constant of the ring as $k = \frac{\Delta P}{\Delta \overline{AB}}$ and the corresponding dimensionless quantity $\bar{k} = \frac{k}{EI/R^3}$. For the CNT ring shown in Fig. 5(a), its spring constant is calculated to be $k = 17.2$ mN/m. We analyze the stiffness of the CNT ring of ring radius ranging between 30 nm and 70 nm, all of which fall into the region above the circle/square curves in Fig. 3(a). The dependence of the ring's spring constant on the ring radius is presented in Fig. 7(a). Our results reveal that the normalized stiffness of the ring ($\bar{k}$) is linearly proportional to the ring radius, and thus the stiffness of the ring in compression is inversely proportional to the square of the ring radius, i.e., $k \sim \frac{EI}{R^2}$. By properly selecting the ring parameters, our work suggests that CNT rings can be used as ultrasensitive force sensors and stretchable and flexible structural components in nanoscale mechanical and electromechanical systems.

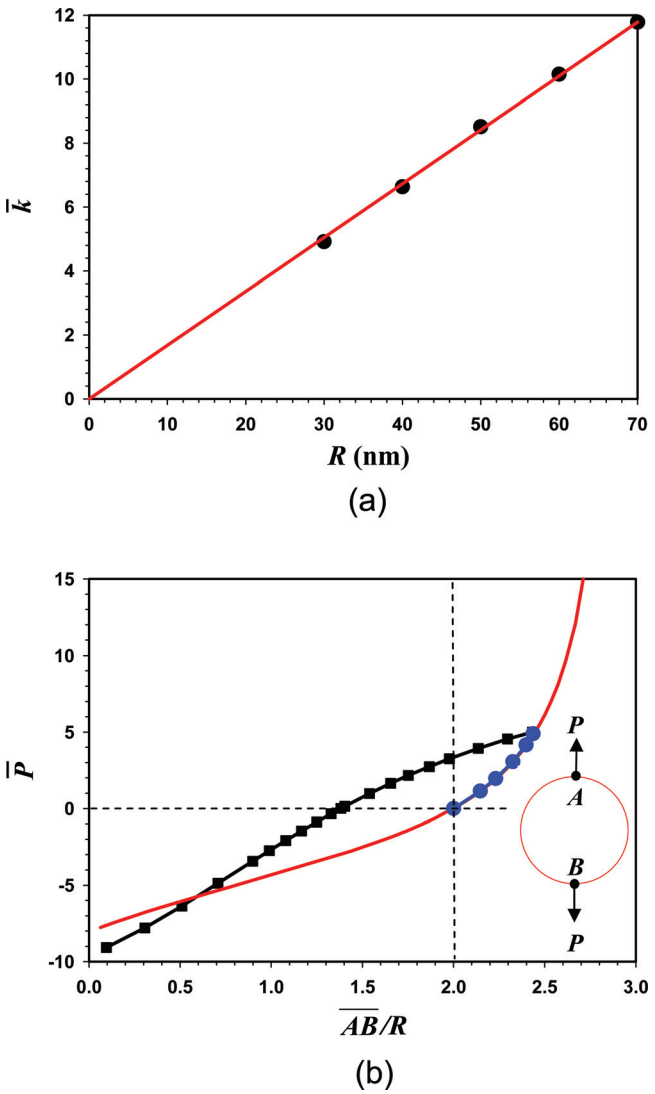

FIG. 7. (Color online) (a) The dependence of the spring constant of CNT rings of initial flat contact with the substrate on the ring radius, (b) The comparison of the force-ring height profile shown in Fig. 6(a) with that of a comparable CNT ring under two point loads as illustrated by the inset (red solid curve).

We examine the effect of the substrate on the mechanical deformation of the CNT ring. Without the substrate, the mechanical deformation of circular ring structures under two balanced point loads is a classical structural mechanics problem and its analytical solutions, based on nonlinear elastica theory, were reported in Ref. 27. The comparison of the mechanical deformations of the CNT ring as shown in Fig. 5(a) with and without the contacting substrate is presented in Fig. 7(b). Our results show that, under tensile loading, the mechanical deformation of the CNT ring without the substrate [solid curve in Fig. 7(b)] overlaps well with the circle branch of the elastic profile of the CNT ring that is in contact with the substrate. In the compressive loading regime, the mechanical deformation profile of the CNT ring under two point loads displays a nonlinear relationship and the slope of the force–ring height profile is smaller than that of the same CNT ring interacting with the substrate. It is noticed that the mechanical deformation of the CNT without the substrate contact displays a monotonous force-deformation relationship under both compressive and tensile loadings. Our results clearly demonstrate that the *vdw* interaction between the CNT ring and the substrate plays an important role in the mechanical behavior of the CNT ring in both tension and compression regimes.

Lastly, we investigate the mechanical deformation of the CNT ring above the graphite sheet when the CNT ring is able to keep a perfectly circular conformation in its relaxed configuration (i.e. without having a flat ring segment). For this purpose, we consider a circular ring made of a thin SWNT bundle, as illustrated in Fig. 8(a). The bundle consists of seven SWNTs, which are assumed to be oriented in a hexagonal configuration. We reasonably assume that the tubes in the bundle retain their circular cross sections during the ring deformation process. The intertube distance, l_0, is given by $l_0 = 2R_{CNT} + 0.313nm$.[34] By considering that the tubes in the bundle are arm-chair SWNTs and two tubes in the bundle are in contact with the substrate, the critical ring radii R_{cr}^{buckle} and R_{cr}^{flat} are calculated using the approaches reported in Sec. II, and are plotted in Fig. 8(b). Our results reveal that the critical ring radius for unbuckled CNT rings [circle curve in Fig. 8(b)] is smaller than that of CNT rings of no flat ring segment in contact with the substrate [square curve in Fig. 8(b)], which is due to the significant increase of the bending stiffness of the nanotube bundle. Here, we only consider the parameters of the CNT ring in the region between the square and circle curves in Fig. 8(b), where the CNT ring preserves its perfectly circular configuration when it stands above a 40-layer graphite substrate. Selected deformation curvatures for a CNT ring, which is made of a bundle consisting of 7 (10,10) tubes and has a radius of 100 nm, are obtained based on the elastica model presented in Sec. II and are presented in Fig. 9(a). The flexural rigidity of this

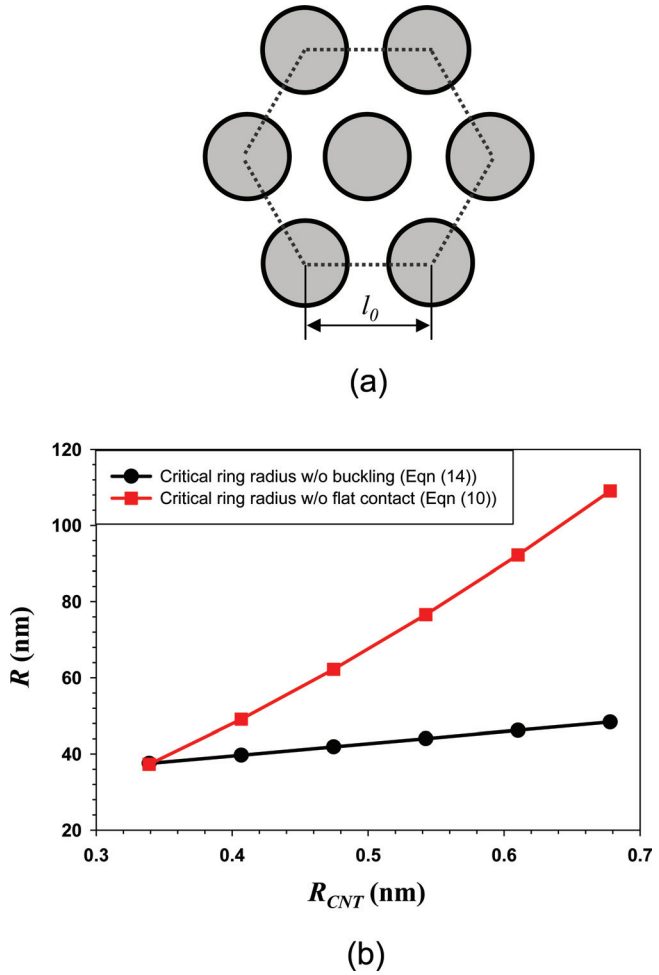

FIG. 8. (Color online) (a) Schematic of the cross section of a bundle consisting of seven identical nanotubes; (b) the respective dependences of the critical ring radii for a bundled-tube-based CNT ring of no flat contact with the substrate (red-square curve) and of no buckling (black-circle curve) on the radius of the individual tubes. The considered nanotube bundle is made of seven arm-chair single-walled carbon nanotubes.

bundled tube is calculated to be 1.36×10^{-23} N·m^2. Figures 9(b) and 9(c) show the respective dependences of the height of the CNT ring and the potential energy in the system on the applied force. Bifurcation is also exhibited in both profiles when the CNT ring is in tension. Similar to earlier discussion, the square curves in both profiles represent the stable deformation curvature while the circle curves represent the unstable deformation curvatures. The differences between both branches of the bifurcation as shown in Figs. 9(b) and 9(c) are much smaller, compared to the respective differences shown in Figs. 6(a) and 6(d). The force–ring height profile of the CNT ring shown in Fig. 9(b) displays a nonlinear relationship in both tension and compression regimes. Figure 9(b) also shows a comparison of the force–ring height profiles for the CNT ring with and without the substrate, the latter of which is shown by the solid curve. Both profiles overlap well in the tension regime. The comparison between the deformation profiles presented in Figs. 6 and 9 suggests that the deformation curvature of the CNT ring on the substrate under external compressive or tensile loadings is highly dependent on relaxed conformation on the substrate.

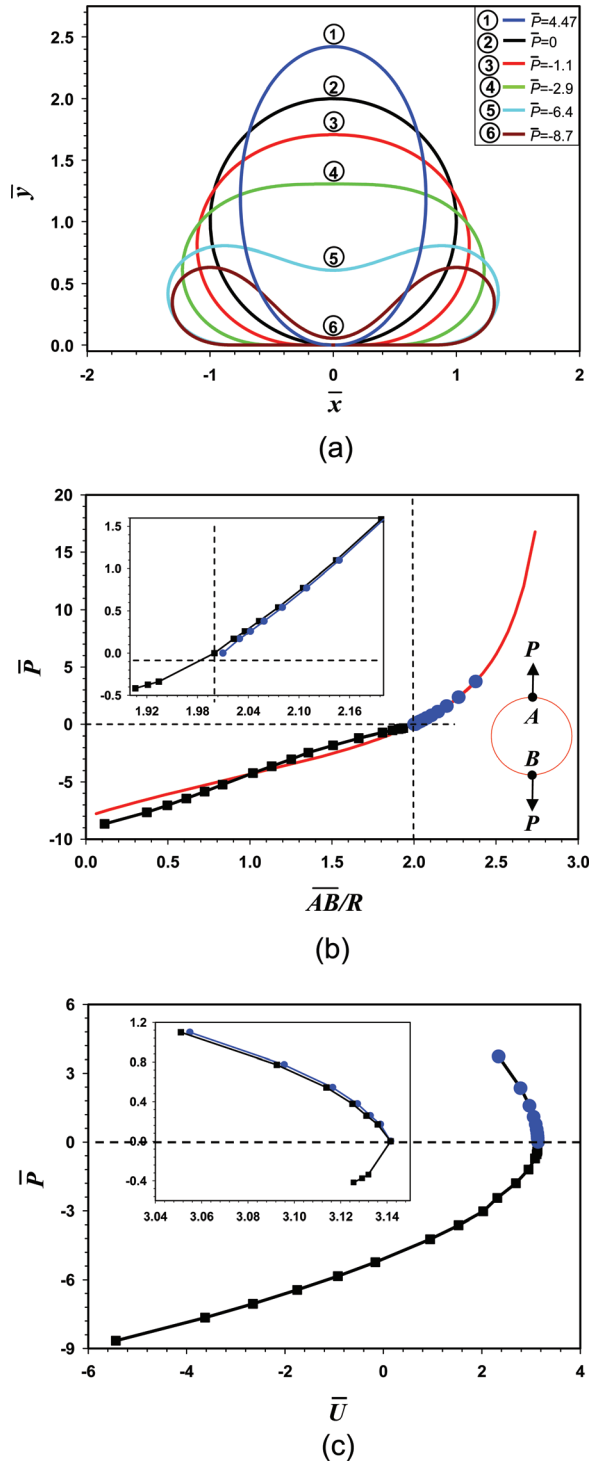

FIG. 9. (Color online) (a) Representative deformation curvatures of the CNT ring, which relaxed conformation on the substrate remains perfectly circular, a variety of tensile and compressive loads; (b) the dependence of the ring height on the applied load (black-square and blue-circle curves) and its comparison with the deformation profile for a comparable CNT ring under two point loads as illustrated by the inset (red-solid curve); (c) the dependence of the total potential energy in the system on the applied load.

IV. CONCLUSION

In this paper, the elastic deformations of the CNT ring on a flat substrate under a variety of external loading conditions are investigated using a nonlinear continuum elastica model. Our results clearly reveal that the *vdw* interaction

between the CNT ring and the substrate has profound effects on its deformation curvature. Our results show that the load-deformation profiles of the CNT ring under tensile loading exhibit bifurcation behavior, which is ascribed to its *vdw* interaction with the substrate. The mechanical deformation of the CNT ring on the graphite surface is also dependent on its relaxed conformation, which is determined by its stiffness and *vdw* interaction with the substrate. Our work suggests that CNT rings are promising for a number of applications, such as ultrasensitive force sensors and stretchable and flexible structural components in nanoscale mechanical and electromechanical systems.

ACKNOWLEDGMENTS

This work was supported by the State University of New York at Binghamton, and was partially supported by the American Chemical Society–Petroleum Research Fund.

[1]J. Liu, H. J. Dai, J. H. Hafner, D. T. Colbert, R. E. Smalley, S. J. Tans, and C. Dekker, Nature **385**, 780, 1997.
[2]Z. P. Zhou, D. Y. Wan, Y. Bai, X. Y. Dou, L. Song, W. Y. Zhou, Y. J. Mo, and S. S. Xie, Physica E (Amsterdam) **33** 24, 2006.
[3]M. J. Buehler, Y. Kong, and H. J. Gao, J. Eng. Mater. Technol. Trans. ASME **126**, 245, 2004.
[4]M. J. Buehler, Y. Kong, H. Gao, and Y. Huang, J. Eng. Mater. Technol. Trans. ASME **128**, 3, 2006.
[5]M. J. Buehler, J. Mater. Res. **21**, 2855, 2006.
[6]M. Sano, A. Kamino, J. Okamura, and S. Shinkai, Science **293**, 1299, 2001.
[7]S. W. Liu, J. J. Zhu, Y. Mastai, I. Felner, and A. Gedanken, Chem. Mater. **12**, 2205, 2000.
[8]R. Martel, H. R. Shea, and P. Avouris, J. Phys. Chem. B **103**, 7551, 1999.
[9]S. L. Zou, D. Maspoch, Y. H. Wang, C. A. Mirkin, and G. C. Schatz,. Nano Lett. **7**, 276, 2007.
[10]Y. H. Wang, D. Maspoch, S. L. Zou, G. C. Schatz, R. E. Smalley, and C. A. Mirkin, Proc. Natl. Acad. Sci. U.S.A. **103**, 2026, 2006.
[11]S. Motavas, B. Omrane, and C. Papadopoulos, Langmuir **25**, pp. 4655, 2009.
[12]D. H. Oh, J. M. Park, and K. S. Kim, Phys. Rev. B **62**, 1600, 2000.
[13]M. Huhtala, A. Kuronen, and K. Kaski, Comput. Phys. Commun. **147**, 91, 2002.
[14]M. Huhtala, A. Kuronen, and K. Kaski,. Comput. Phys. Commun. **146**, 30, 2002.
[15]P. Liu, Y. W. Zhang, and C. Lu, Phys. Rev. B **72**, 115408, 2005.
[16]O. Hod, E. Rabani, and R. Baer, Phys. Rev. B **67**, 195408, 2003.
[17]J. Han, Chemical Phys. Lett. **282**, 187, 1998.
[18]L. Liu, C. S. Jayanthi, and S. Y. Wu, Phys. Rev. B **6403**, 033412, 2001.
[19]C. Feng and K. M. Liew, Carbon **47**, 3508, 2009.
[20]V. Meunier, P. Lambin, and A. A. Lucas, Phys. Rev. B **57**, 14886, 1998.
[21]S. L. Zhang, S. M. Zhao, M. G. Xia, E. H. Zhang, and T. Xu, Phys. Rev. B, **68**, 7, 2003.
[22]M. Zheng and C. Ke, Small **6**, 1647, 2010.
[23]Y. Mikata, Acta Mech. **190**, 133, 2007.
[24]C. Ke, M. Zheng, G. Zhou, W. Cui, N. Pugno, and R. N. Miles, Small **6**, 438, 2010.
[25]C.-H. Ke, M. Zheng, and I.-T. Bae, and G.-W. Zhou, J. Appl. Phys. **107**, 104305, 2010.
[26]M. R. Falvo, G. J. Clary, R. M. Taylor, V. Chi, F. P. Brooks, S. Washburn, and R. Superfine, Nature **389**, 582, 1997.
[27]R. Frisch-Fay, *Flexible Bars* (Butterworths, London, 1962).
[28]M. Dequesnes, Z. Tang, and N. R. Aluru,. J. Eng. Mater. Technol. Trans. ASME **126**, 230, 2004.
[29]T. Tang, A. Jagota, and C. Y. Hui, J. Appl. Phys., **97**, 074304, 2005.
[30]L. D. Landau and E. M. Lifshitz, *Theory of Elasticity* 3rd ed. Pergamon Press 1986.
[31]O. A. Goussev, P. Richner, and U. W. Suter, J. Adhes. **69**, 1, 1999.
[32]T. Hertel, R. E. Walkup, and P. Avouris, Phys. Rev. B **58**, 13870, 1998.
[33]C. Feng and K. M. Liew, Carbon **47**, 1664, 2009.
[34]L. A. Girifalco, M. Hodak, and R. S. Lee, Phys. Rev. B **62**, 13104, 2000.
[35]M. S. Dresselhaus, G. Dresselaus, and P. Avouris, *Carbon Nanotubes* (Springer, Berlin, 2001).
[36]A. N. Kolmogorov and V. H. Crespi, Phys. Rev. B, **71**, 235415, 2005.
[37]C. H. Kiang, M. Endo, P. M. Ajayan, G. Dresselhaus, and M. S. Dresselhaus, Phys. Rev. Lett. **81**, 1869, 1998.